PNAS
www.pnas.org

Supplementary Information for

Coiled-coil 1-mediated fastening of the neck and motor domains for kinesin-3 autoinhibition

Jinqi Ren, Shuang Wang, Han Chen, Wenjuan Wang, Lin Huo, and Wei Feng

Wei Feng
Email: wfeng@ibp.ac.cn

This PDF file includes:

www.pnas.org/cgi/doi/10.1073/pnas.1811209115

Supplementary Information Text

Materials and Methods

Limited proteolysis assay

The wild type and various mutants of the MD-NC-CC1 tandem of KIF13B (~1 mg/ml) were digested by Proteases K (~2 μg/ml) in 50 mM Tris-HCl, pH 7.5, 150 mM NaCl, 2 mM $MgCl_2$, 1 mM EGTA, 1 mM DTT at 25 °C. The reactions were terminated at several time points (0, 10, 20, 30, 45, 60 min) by adding phenylmethanesulfonyl fluoride (PMSF) into the reaction system and the protein samples were then analyzed by SDS-PAGE.

Circular dichroism (CD) analysis

CD analysis of the MD-NC-CC1 tandem of KIF13B and the various mutants was performed on a Chirascan Plus (Applied Photo Physics) spectrometer using a 10 mm pathlength cell. The protein samples (~0.15 mg/ml) were in the buffer containing 50 mM Tris-HCl, pH 7.5, 20 mM NaCl, 2 mM $MgCl_2$, 1 mM EGTA, 1 mM DTT. The CD spectra were recorded from 260 nm to 200 nm at 25 °C.

***In vitro* microtubule-binding assay**

All the protein samples were centrifuged at 100,000 g for 20 min to remove any non-functional fractions. And then the protein samples were incubated with pre-assembled microtubules (Cytoskeleton, Inc.) for 5 min at 25 °C in the buffer containing 80 mM PIPES, pH 6.9, 50 mM NaCl, 1 mM EGTA, 2 mM $MgCl_2$, 0.25% (v/v) Tween-20 and 0.1 mM Taxol. The mixtures were then subjected to centrifugation at 100,000 g for 10 min at 25 °C. The pellet and supernatant fractions were analyzed by SDS-PAGE. Bovine serum albumin (BSA) was used as the control.

Molecular dynamics simulations

The initial simulation model of the MD-NC-CC1-Y73C mutant was built by adding the missing loop using Modloop server (1). The modeled structure was then solvated in a 99×120×90 $Å^3$ water box and 54 Na^+/47 Cl^- were added to neutralize the system. The NAMD package (2) and amber ff14SB all atom force field (3) were used for energy minimizations

and molecular dynamics simulations. The parameters of the ATP/ADP molecules are from Carlson's group (4). Under periodic boundary conditions, a 10 Å cutoff was used for van der Waals interactions and Particle Mesh Ewald summation was used to calculate the electrostatic interactions. For each simulation, energy was first carefully minimized to avoid any possible clashes. The energy-minimized system was then equilibrated for 5 ns with temperature controlled at 310K by Langevin dynamics and pressure controlled at 1 atm by the Langevin piston method. With the equilibrated structure, 50 ns free dynamics simulations were performed. In the simulations, SHAKE method was used on all hydrogen-containing bonds to allow a 2 fs time step. The trajectories were analyzed with VMD program (5).

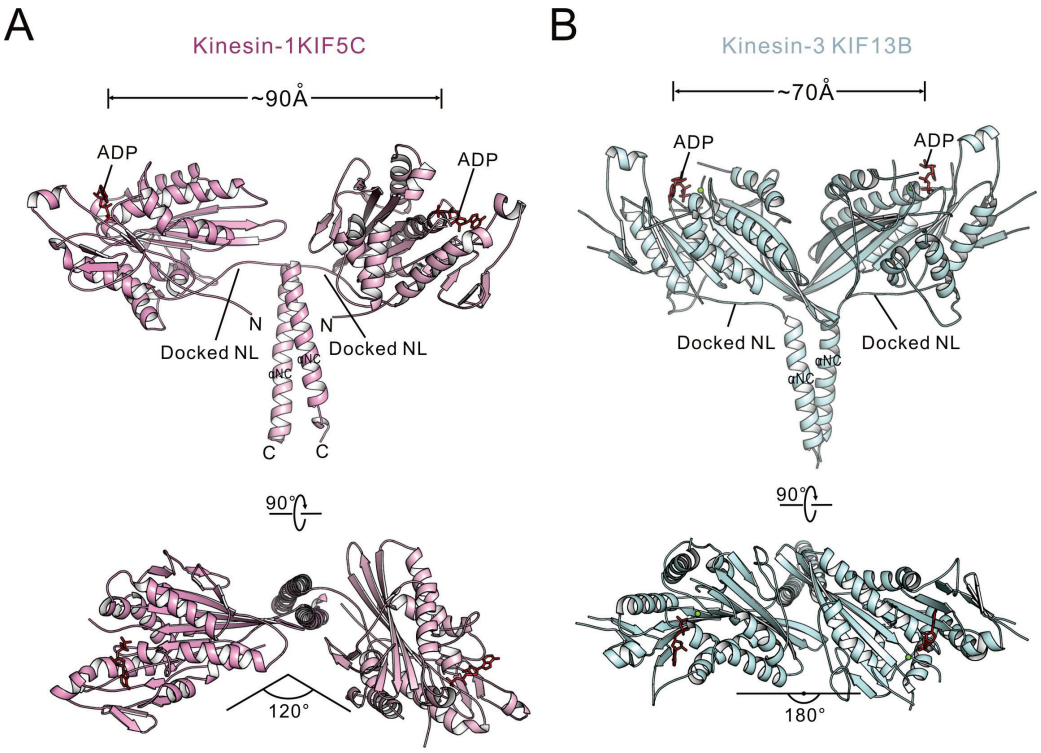

Fig. S1. Structural comparison of the MD-NC dimers of kinesin-1 and kinesin-3. The structures of the MD-NC dimers of kinesin-1 (PDB code: 3KIN) (A) and kinesin-3 determined in this study (B) are shown in the ribbon representation and colored in pink and pale-cyan, respectively. In the two dimer structures, NL docks on the motor domain. Based on the distance between the nucleotide-binding pockets of the two motor domains, the distance between the two domains of kinesin-1 and kinesin-3 is different, i.e., ~90 Å in kinesin-1 *v.s.* ~70 Å in kinesin-3.

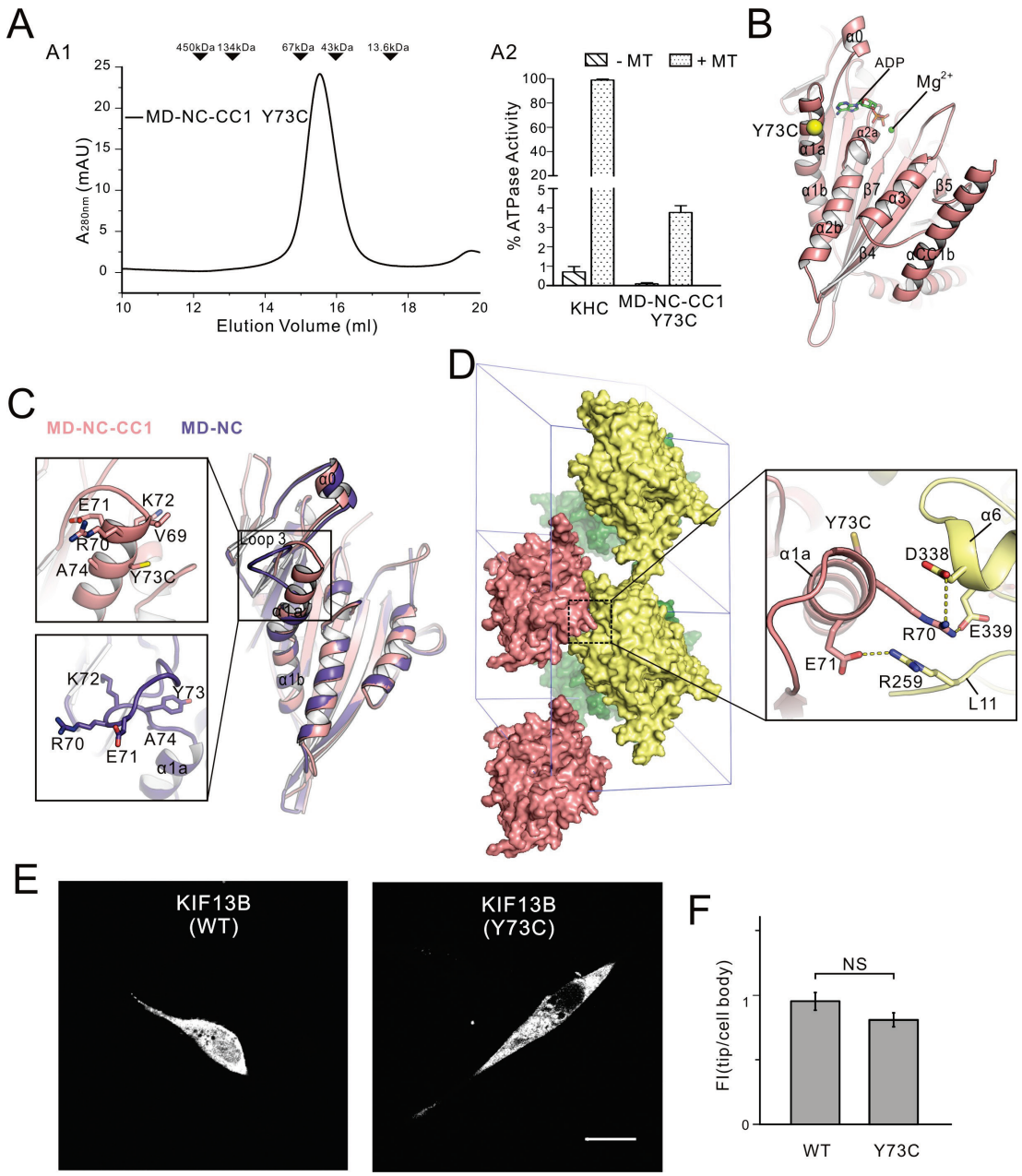

Fig. S2. The Y73C mutation does not interfere with the monomeric inhibited state of the MD-NC-CC1 tandem but facilitates the crystal packing. (*A*) Biochemical characterization of MD-NC-CC1-Y73C mutant. Both the analytical gel-filtration analysis (A1) and MT-stimulated ATPase assay (A2) showed that the Y73C mutant adopts a monomeric inhibited state similarly to the wild type. **(*B*)** A ribbon diagram of the MD-NC-CC1-Y73C structure. The Y73C mutation is marked. **(*C*)** Structural comparison of the MD-NC and MD-NC-CC1-Y73C structures demonstrated that the Y73C mutation only induces the local conformational changes in loop 3 of the motor domain. The Y73C mutation extends the following helix α1a and stabilizes loop 3 of the motor domain. **(*D*)** Crystal packing analysis of the MD-NC-CC1-Y73C mutant. The extended helix α1a happens to sit at the intermolecular packing interface of the crystal and makes the extensive contacts with the neighboring molecule to facilitate the crystal packing. **(*E*)** Cellular localizations of the full-length KIF13B and the Y73C mutant in the N2A cells. Scale bar: 20 μm. **(*F*)**

Quantification of the cellular distribution data shown in panel E. The ratio of the tip to cell body average fluorescence intensity (FI) was quantified for each construct for more than 15 cells (n > 15). Each bar represents the mean value ±SEM. NS: no significant differences.

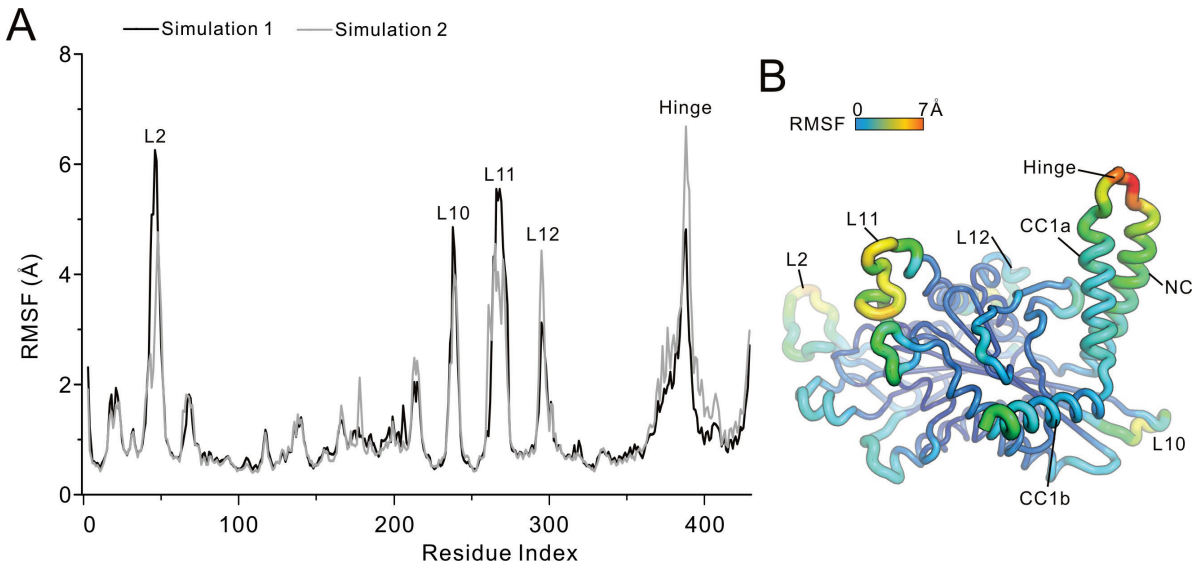

Fig. S3. Molecular dynamics simulations of the MD-NC-CC1-Y73C structure. (*A*) The root-mean-square-fluctuations (RMSF) for each residue in the MD-NC-CC1-Y73C structure were plotted**.** Results of the two independently simulations were shown. Four flexible loops (loop 2 and loop 10-12) in the motor domain and the NC/CC1 hinge region that exhibit the highly dynamic conformations were labeled. **(*B*)** A sausage-style cartoon diagram showing the root-mean-square-fluctuation (RMSF) of the MD-NC-CC1-Y73C structure during the molecular dynamics simulations. Different regions of the structure are colored according to their RMSF values.

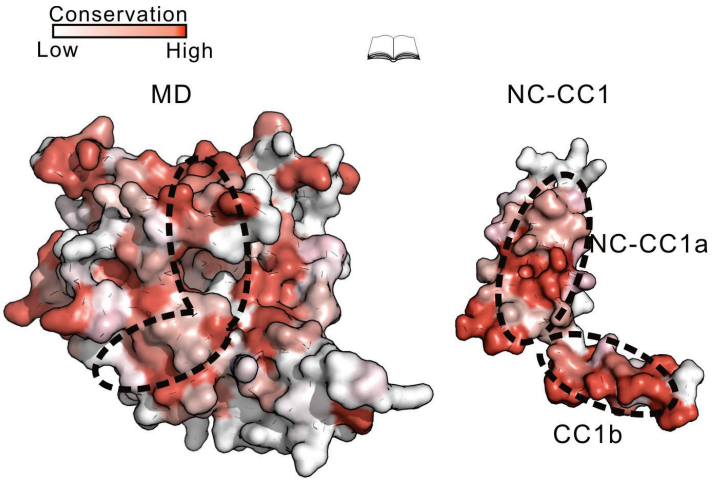

Fig. S4. An "open-book" view of the MD-NC-CC1-Y73C structure in a surface representation. The surface is colored according to the sequence conservation of KIF13B in different species. The interaction interface between the motor domain and NC-CC1 is also marked.

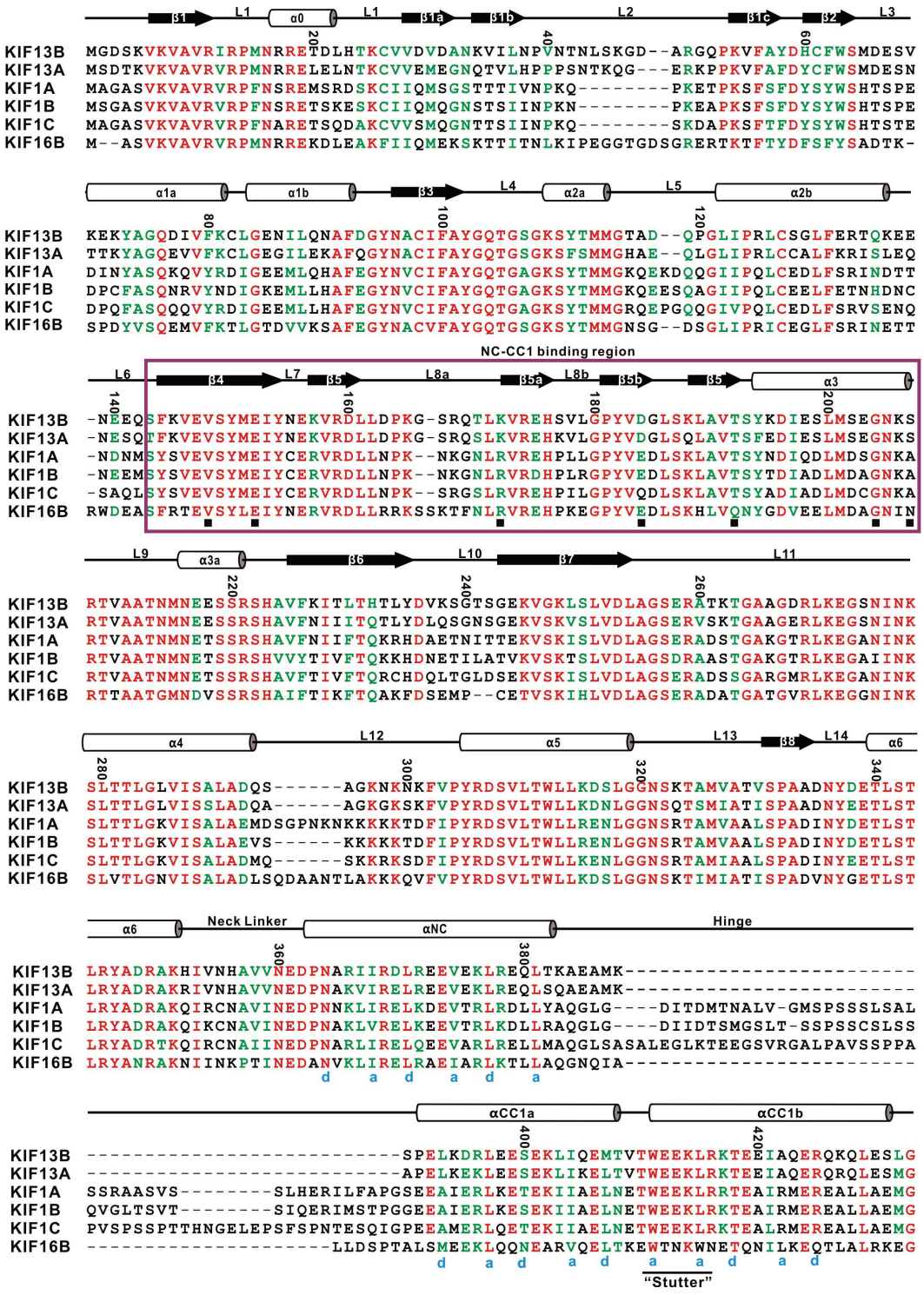

Fig. S5. Structure-based sequence alignment of the MD-NC-CC1 regions of different kinesin-3 motors from human. The identical residues and highly conserved residues are colored in red and green, respectively. The residue numbers and secondary structures of KIF13B are marked at the top. The NC-CC1-binding region in the motor domain is highlighted by a brown box. The disease-related point mutations in the NC-CC1-binding region of KIF1A (V144F, E148D, R167C, E179G, T187I, G199R and A202P) are marked with black squares at the bottom. The *a* and *d* sites of the heptad repeat pattern of NC and CC1 are also labeled.

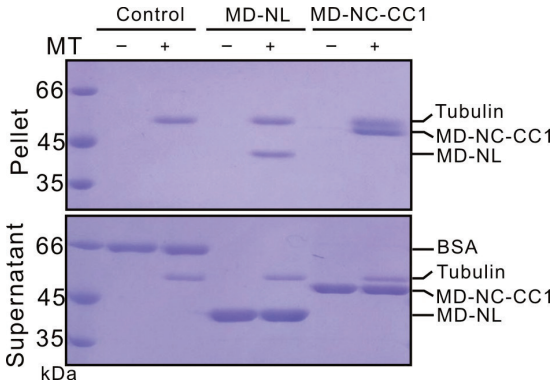

Fig. S6. The microtubule-binding capacities of the motor domain (with NL) and the MD-NC-CC1 tandem. *In vitro* microtubule-binding assay of the MD-NL and MD-NC-CC1 tandems. Both the MD-NL and MD-NC-CC1 tandems can bind to microtubules. The bovine serum albumin (BSA) was used as the control.

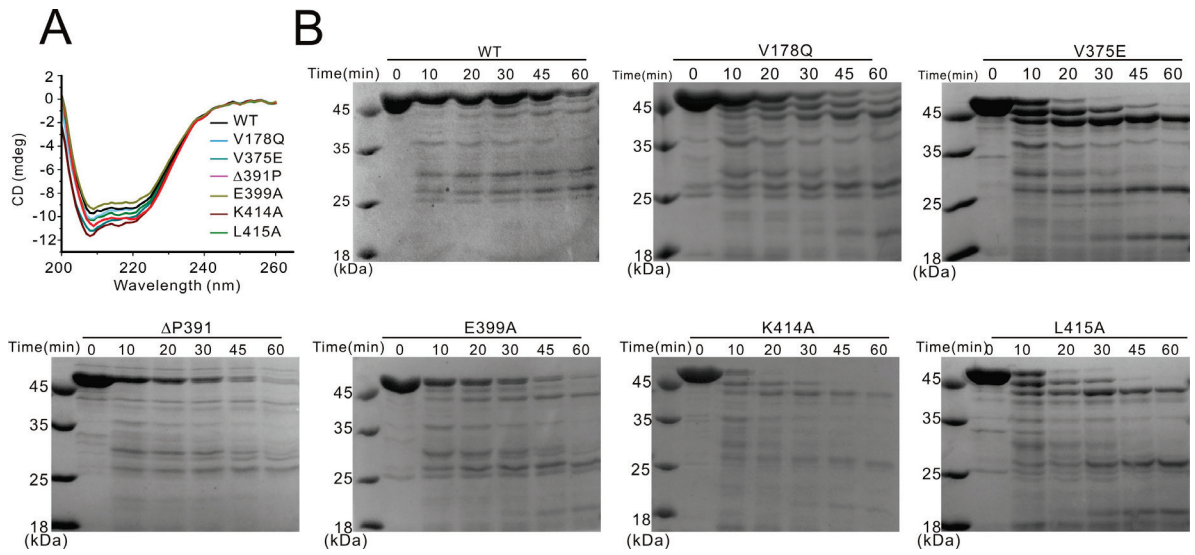

Fig. S7. Biochemical characterization of the wild type and various mutants of the MD-NC-CC1 tandem of KIF13B. (*A*) The CD spectra of the wild type and various mutants of the MD-NC-CC1 tandem of KIF13B. The data showed that all the mutations do not have major effects on the secondary structures of the MD-NC-CC1 tandem. **(*B*)** The limited proteolysis assay of the wild type and various mutants of the MD-NC-CC1 tandem of KIF13B. Most of the mutations destabilize the MD-NC-CC1 tandem.

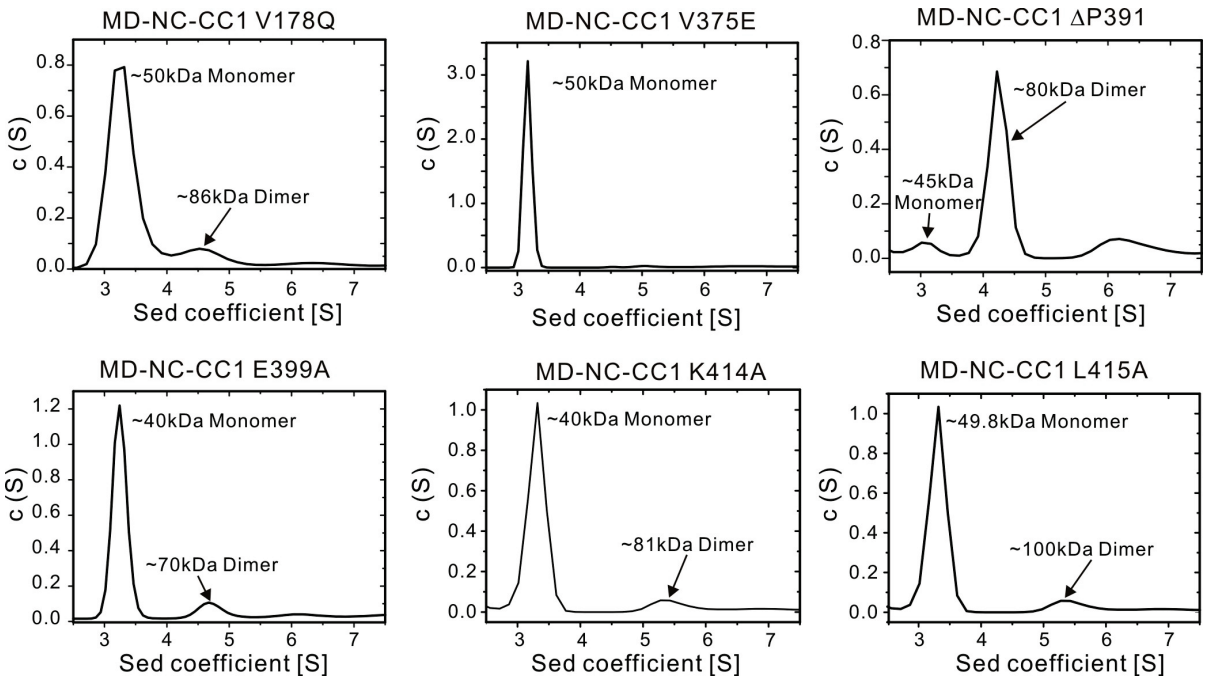

Fig. S8: Analytical ultracentrifugation analysis of various mutants of the MD-NC-CC1 tandem. The calculated molecular mass for each mutant is labeled in each panel. The ΔP391-mutant adopts a dimeric conformation and the V178Q, E399A, K414A and L415A mutants exist in a monomer/dimer equilibrium in solution. The V375E-mutant (with mutation in NC) remains as a monomer.

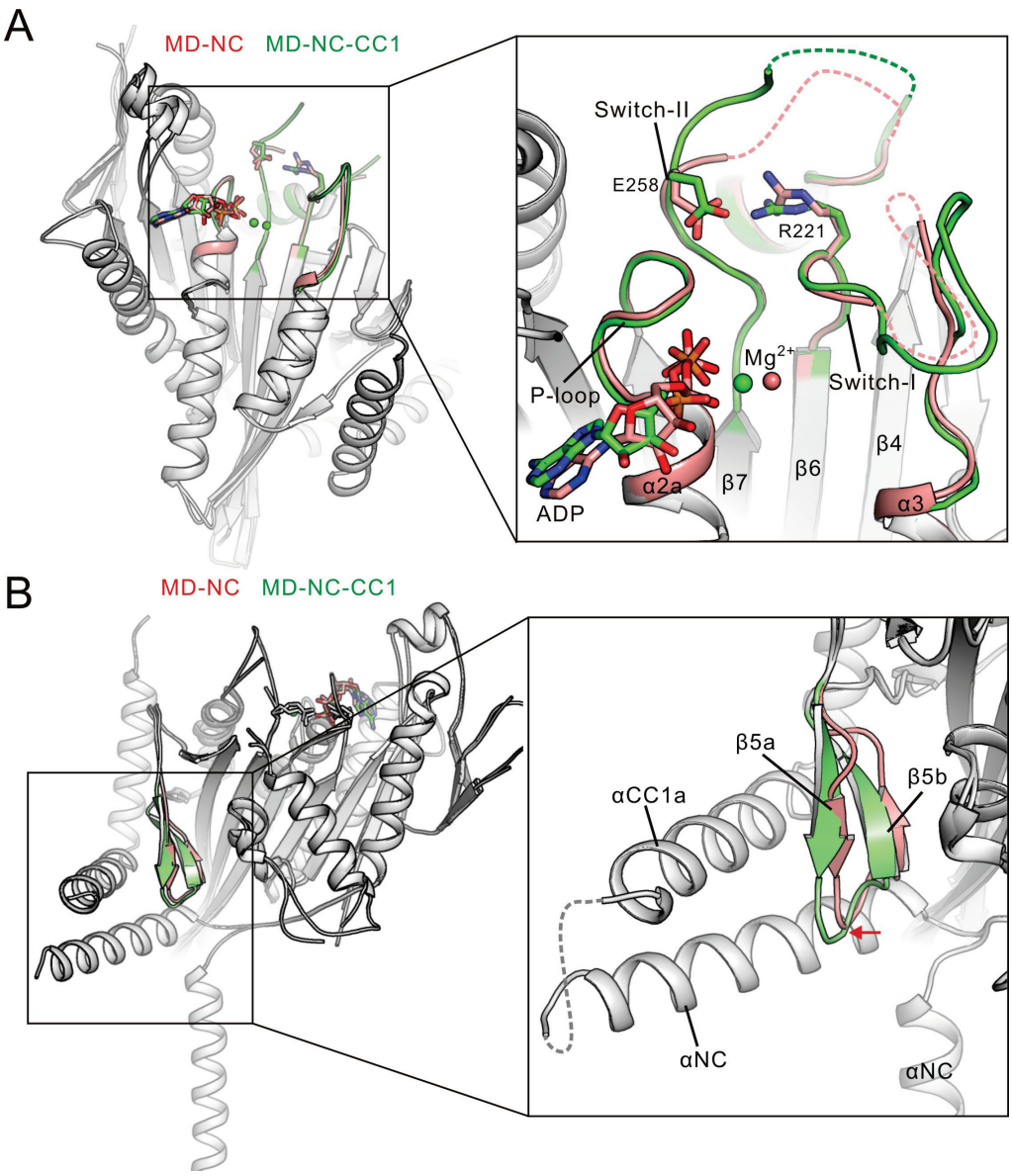

Fig. S9. Structural comparison of the motor domains from the MD-NC dimer and the MD-NC-CC1 monomer. The motor domains from the two structures can be well-aligned with each other (with the RMSD of ~0.37 Å for the backbone atoms). Since the two motor domains were both trapped in the similar ADP-bound state, no significant structural changes were found in the Switch I and II elements of the motor domain (A). On the other hand, the binding of the NC-CC1a bundle and CC1b to the motor domain induced some local conformational changes in the β5a/β5b region of the motor domain (B).

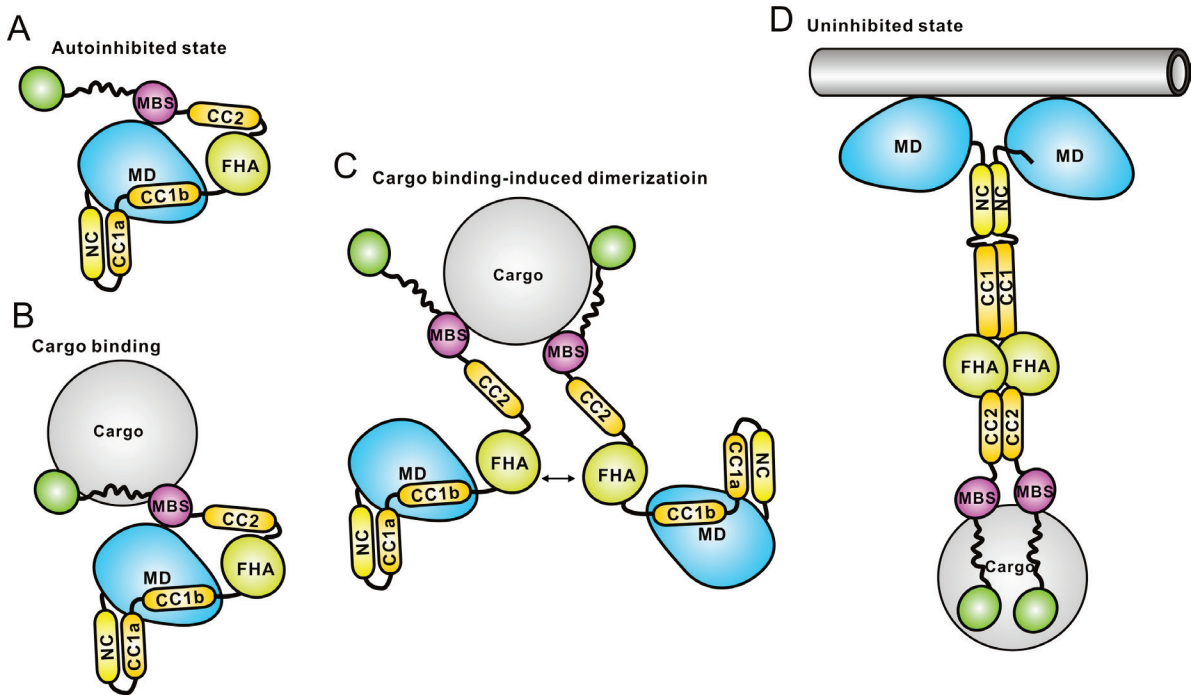

Fig. S10. A schematic working model for the cargo-mediated transition of the full-length KIF13B from an autoinhibited monomer to an uninhibited dimer. In the autoinhibited state (A), CC1 interacts with both NC and the motor domain, CC2 interacts with the FHA domain, and the MBS segment binds to the motor domain. Upon binding to cargoes or cargo adaptors likely through the MBS segment (B), the FHA domain could be somehow released to promote the formation of the CC1-FHA dimer that would further release the CC1-mediated inhibition of the neck domain (C). In the uninhibited state, the FHA domain, CC1 and NC would work together to form a stable dimer that brings the two motor domains together for walking along microtubules (D).

Table S1: Data collection and structural refinement statistics

Data collection		
Data sets	MD-NC	MD-NC-CC1-Y73C
Beam Line	BL19U1	BL17U1
Wavelength(Å)	0.9791	0.9791
Space group	$P3_2\,21$	$P3_2$
Unit cell parameters(Å)	87.4, 87.4, 97.5	75.1, 75.1, 91.7
Resolution range(Å)	39.87-2.58(2.65-2.58)[a]	50.0-2.4(2.53-2.40)
No.of unique reflections	13889(1023)	22223(3271)
Redundancy	18.7(20.0)	3.5(3.6)
I/σ(I)	14.0(1.7)	8.0(1.9)
Rmerge (%)[b]	6.2(66.5)	9.7(61.5)
Completeness (%)	99.4(99.7)	98.3(98.6)
Structure refinement		
Resolution (Å)	39.87-2.58(2.70-2.58)	50.0 - 2.40 (2.24-2.40)
Rwork(%)[c]	23.8(35.5)	19.3(27.7)
Rfree(%)[d]	28.6(43.2)	24.9(34.7)
R.M.S.D bonds (Å)	0.009	0.002
R.M.S.D angles (º)	1.119	0.602
Average B factor	63.1	61.1
Ramachandran plot(%)		
Favored regions	96.0	95.7
Allowed regions	4.0	4.3
Disallowed regions	0.0	0.0

[a]The values in parentheses refer to the highest resolution shell.

[b]$R_{merge}=\sum_h\sum_i|I_i(h) - \langle I(h)\rangle|/\sum_h\sum_i I_i(h)$, where I is the observed intensity and $\langle I\rangle$ is the average intensity of multiple observations of symmetry-related reflection h.

[c]R_{work} is the $R_{factor}$for the working dataset. $R_{factor}=\sum||Fo|-|Fc||/\sum|Fo|$ where $|Fo|$ and $|Fc|$ are observed and calculated structure factor amplitudes respectively.

[d]R_{free} is the cross-validation R_{factor} computed for a randomly chosen subset of 5% of the total number of reflections, which were not used during refinement.

Table S2: MT-stimulated mant-ADP release rates

Construct	–MT (s^{-1})	+MT(s^{-1})
MD	0.07±0.00	3.59±0.08
MD-NC-CC1 WT	0.06± 0.00	0.14 ±0.01
MD-NC-CC1 V375E	0.09± 0.00	0.73± 0.01
MD-NC-CC1 ΔP391	0.11± 0.00	4.03± 0.13
MD-NC-CC1 L415A	0.11± 0.01	1.20±0.02

*Data are represented as the mean value ±SD. –MT and +MT: microtubules are either present (+) or absent (–) in the measurement.

References:

1. Fiser A & Sali A (2003) ModLoop: automated modeling of loops in protein structures. *Bioinformatics* 19:2500-2501.
2. Phillips JC*, et al.* (2005) Scalable Molecular Dynamics with NAMD. *J. Comput. Chem.* 26:1781-1802.
3. Maier JA*, et al.* (2015) ff14SB: Improving the Accuracy of Protein Side Chain and Backbone Parameters from ff99SB. *J. Chem. Theory Comput. 2015, 11,* 11:3696-3713.
4. Meagher KL, Redman LT, & Carlson HA (2003) Development of polyphosphate parameters for use with the AMBER force field. *J Comput Chem* 24:1016-1025.
5. Humphrey W, Dalke A, & Schulten K (1996) VMD: Visual molecular dynamics. *J. Mol. Graph.* 14:33-38.